Nanoscale

Accepted Manuscript

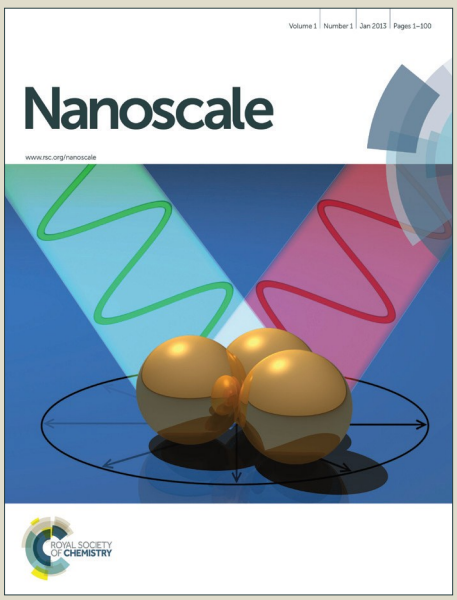

This is an *Accepted Manuscript*, which has been through the Royal Society of Chemistry peer review process and has been accepted for publication.

Accepted Manuscripts are published online shortly after acceptance, before technical editing, formatting and proof reading. Using this free service, authors can make their results available to the community, in citable form, before we publish the edited article. We will replace this *Accepted Manuscript* with the edited and formatted *Advance Article* as soon as it is available.

You can find more information about *Accepted Manuscripts* in the Information for Authors.

Please note that technical editing may introduce minor changes to the text and/or graphics, which may alter content. The journal's standard Terms & Conditions and the Ethical guidelines still apply. In no event shall the Royal Society of Chemistry be held responsible for any errors or omissions in this *Accepted Manuscript* or any consequences arising from the use of any information it contains.

ROYAL SOCIETY OF CHEMISTRY

www.rsc.org/nanoscale

Cite this: DOI: 10.1039/c0xx00000x

www.rsc.org/xxxxxx

ARTICLE TYPE

Si/Ag Composite Building by Interconnected Micro-Nano Bimodal Porous Structure as High-Performance Anode for Li-Ion Batteries

Qin Hao, Dianyun Zhao, Huimei Duan, Qiuxia Zhou and Caixia Xu*

Received (in XXX, XXX) Xth XXXXXXXXX 20XX, Accepted Xth XXXXXXXXX 20XX

DOI: 10.1039/b000000x

A one-step dealloying method is employed to conveniently fabricate bimodal porous (BP) Si/Ag composite in high throughput under mild condition. Upon dealloying the carefully designed SiAgAl ternary alloy in HCl solution at room temperature, the obtained Si/Ag composite has a uniform bicontinuous porous structure in three dimensions with micro-nano bimodal pore size distribution. Compared with the traditional preparation methods for porous Si and Si-based composites, this dealloying route is easy operating and environmentally benign. More importantly, it is convenient to realize the controllable component and uniform distribution of Si and Ag in the product. Owing to the rich porosity of the unique BP structure and incorporation of well conductive Ag, the as-made Si/Ag composite possesses the improved conductivity and alleviated volume changes of Si network during the repeating charging and discharging process. As expected, the BP Si/Ag anode exhibits high capacity, excellent cycling reversibility, long cycling life and good rate capability for lithium storage. When the current rate is up to 1 A g^{-1}, BP Si/Ag can deliver a stable reversible capacity above 1000 mA h g^{-1}, and exhibits a capacity retention up to 89.2 % against the highest capacity after 200 cycles. With the advantages of unique performance and easy preparation, the BP Si/Ag composite holds great application potential as an advanced anode material for Li-ion batteries.

1. Introduction

Li-ion batteries (LIBs) have been widespread employed as power supply in portable electronics and mobile communication devices.[1,2] At present, graphite-like materials represent the class of main anode materials in commercialized LIBs, however, a low theoretical capacity of 372 mA h g^{-1} for these materials has limited the broad development of LIBs to meet the ever increasing requirements for high power sources.[3] Therefore, great efforts have been made to explore highly efficient anode materials in terms of high capacity, high energy density, and long cycling life. As so far, a variety of anode materials for LIBs have been reported, such as metal oxides, tin-based and silicon-based materials, etc.[4] Among these materials, silicon has received growing attentions as promising alternative anode material with the advantages of the theoretical capacity as high as 4200 mA h g^{-1} and low discharge potential. However, its low electric conductivity and large volume changes owing to Li alloying and dealloying reactions commonly cause the serious capacity degradation, especially at high current densities.[5,6]

In order to solve these problems of silicon anode materials, introducing a well-conductive coating material to modify the electric connectivity of Si is one of effective strategies to improve their electrochemical performances.[7-10] Among various coating materials, Ag has attracted great attentions due to its excellent electric conductivity and negligible effects on the lithium storage behaviors of Si.[11-15] In addition, the development of Si nanomaterials with desirable morphologies has been used to alleviate the large volume changes of Si.[16-18] Compared with bulky Si anodes, nanostructured Si has a shorter Li^+ diffusion distance and higher electroactivity, meanwhile, the nanostructure is beneficial for relieving the absolute volume variation from lithiation. Compared with Si nanomaterials, bulky Si materials can be packed more densely on the current collector against collapse, and have the higher volumetric energy density and fewer undesirable surface reactions due to the low surface areas.[19,20] Consequently, it is essential to achieve the optimized performance of Si anode by engineering its morphology coupled with the advantages of microscaled and nanoscaled Si materials as well as incorporating well conductive species.

Inspired by the stated above, in current work we focus on designing Si/Ag nanoporous composite with microscaled structure in three dimensions. Although many methods have been explored for preparing porous Si, realizing a controllable and convenient synthesis still remains a great challenge. For example, a magnesiothermic reduction method of SiO_2 was successfully employed to obtain porous Si materials, but the process required an oxygen-free environment and a high temperature,[21] while the dominant Si etching techniques always need fluorine-based solutions, which is unfriendly considering the green synthesis.[22,23] Meanwhile, the Ag nanoparticles of the Si/Ag composites were mainly introduced by silver mirror reaction using toxic organics as reductants,[12,13] such as aldehydes. Therefore, it is preferable to use a simple and environmentally benign method to fabricate the

Nanoscale Accepted Manuscript

expected Si/Ag composite. Dealloying method has demonstrated to be a powerful and versatile technique for preparing porous metal materials by careful design of the source precursor alloys.[24,25] More importantly, the as-made samples represent an interesting class of bulky microscaled materials with interconnected hollow channels and nanoscaled backbone run through along all three dimensions.

Herein, a simple one-step dealloying method is employed to fabricate bimodal porous (BP) Si/Ag composite in high throughput under mild condition. The Si/Ag product presents an open bicontinuous network structure with micro-nano bimodal pore size distribution upon dealloying the carefully designed SiAgAl ternary alloy in HCl solution. It is noteworthy that this simple approach is easy to realize the controllable component and the uniform distribution of Si and Ag in the Si/Ag product. The rich porosity and incorporation of well conductive Ag are beneficial for improving the conductivity of Si and alleviating the volume changes during the repeating charge and discharge cycles. As expected, electrochemical measurements demonstrate that the as-made BP Si/Ag composite has the high capacity, excellent cycling reversibility, long cycling life and good rate capability for lithium storage.

2. Experimental Section

2.1 Sample preparation

$Si_{10}Al_{90}$ and $Si_8Ag_2Al_{90}$ (atomic percentage) alloy foils with ~50 mm in thickness were prepared by refining pure (> 99.99 %) Si, Ag, and Al in medium frequency induction furnace, respectively, followed by melt-spinning at 1600 r under a protective argon atmosphere. $Si_{10}Al_{90}$ and $Si_8Ag_2Al_{90}$ were selectively etched in 0.1 mol L^{-1} HCl solutions at room temperature for 10 h, respectively. Finally, the products were washed several times with ultra-pure water (18.2 M Ohm) and dried at room temperature in air.

2.2 Characterization

Powder X-ray diffraction (XRD) was carried out with a Bruker D8 advanced X-ray diffractometer using Cu Ka radiation at a step rate of 0.04 $°s^{-1}$. The morphology and structure of the product were observed through field emission scanning electron microscopy (SEM, JEOL JSM-7600F) with an energy-dispersive X-ray spectrometer (EDS) for compositional analysis. The elemental mapping was obtained using a FEI QUANTA FEG250 scanning electron microscope equipped with an INCA Energy X-MAX-50 X-ray spectroscopy analyzer. High resolution transmission electron microscopy (HRTEM) images were obtained with a JEM-2100 high resolution transmission electron microscope (200 kV). Surface structural properties of the BP-SiAg composite was analyzed by means of an X-ray photoelectron spectrometer (XPS, ESCALab250), using a monochromatized MgKa X-ray as the excitation source and choosing C1s (284.60 eV) as the reference line. The surface areas and pore sizes were measured using a Quadrasorb SI-MP Surface Area and Pore Size Analyzer (Quantachrome Instruments) using the Brunauer-Emmett-Teller (BET) method.

2.3 Electrochemical tests

The electrochemical behavior versus Li was measured using coin-type cells (size: 2032). To prepare the working electrodes, the active Si or Si/Ag powders, acetylene black and sodium alginate were mixed in a weight ratio of 7:1.5:1.5 in ultrapure water. After the slurry was mixed uniformly, it was coated onto a piece of Cu foil and dried under vacuum at 80 ^oC for 12 h. The separator was a Celgard 2300 microporous membrane. The electrolyte was composed of 1 mol L^{-1} $LiPF_6$ dissolved in ethylene carbonate (EC)-dimethyl carbonate (DMC)-ethylene methyl carbonate (EMC) with the volume ratio of 1:1:1. The cells were constructed in an Ar filled humidity-free glove box. The cells were cycled galvanostatically between 0.01 and 3 V using a NEWARE BTS 5V-50 mA computer-controlled galvanostat (Shenzhen, China) at different rates at room temperature. The gravimetric capacities are based on per gram of Si. Electrochemical impedance spectroscopy (EIS) was carried out using a Princeton Applied Research spectrometer by applying an alternating current voltage of 10 mV in the frequency range from 0.01 to 100 kHz.

3. Results and Discussions

To achieve a simple and controllable preparation for porous Si/Ag composite, SiAgAl ternary alloy was selected as the source precursor. First, Al has a rich supply with relatively low price, thus greatly reducing the alloy fabrication cost. Considering basic electrolyte such as NaOH solution can react with Si, hydrochloric acid solution was selected as electrolyte to dealloy the source alloy as well to protect Si and Ag from corrosion and loss. In addition, to verify the influence of the incorporation of well conductive Ag on the electrochemical properties of Si electrode, we also fabricated porous Si material through dealloying SiAl binary alloy.

Fig. 1 presents the resulted structure by dealloying $Si_8Ag_2Al_{90}$ alloy in 0.1 M HCl solution for 10 h at room temperature. As illustrated in the surface scanning electron microscopy (SEM) image (Fig. 1a), the selective corrosion of Al had successfully generated a bulky porous structure with the large pores around 1 μm in diameter distributed on the surface. A higher magnification SEM image (Fig. 1b) displays its more detailed structure. It is interesting to find that in every large pore there is a second-order nanoporous structure formed with the uniform pore/ligament distribution. In addition, a number of nanoparticles with the diameter around 100 nm uniformly dispersed on the porous surface. Due to the microscaled structure size in three dimensions, in the element mapping image Si and Ag elements are uniformly dispersed in the Si/Ag product because of the element overlapping (Fig. 1c&d).

Nanoscale Accepted Manuscript

This journal is © The Royal Society of Chemistry [year]

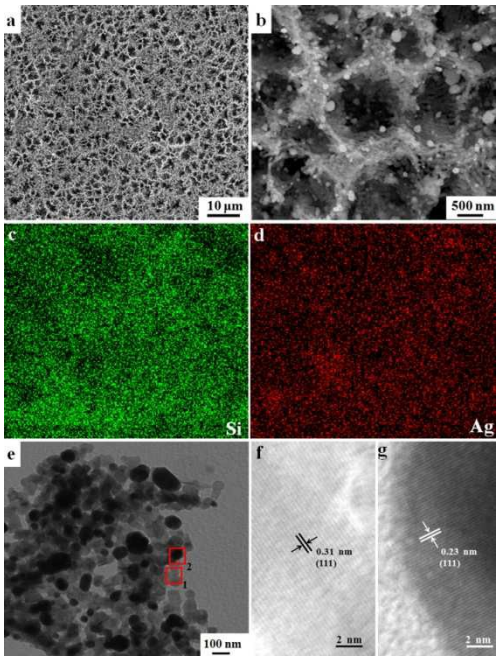

Fig. 1 (a,b) The SEM images, (c,d) elemental mapping, and (e,f) HRTEM images of the BP-Si/Ag composite by dealloying $Si_8Ag_2Al_{90}$ alloy in 0.1 M HCl solution for 10 h at room temperature.

Transmission electron microscopy (TEM) measurement was carried out to further understand this structure. As shown in Fig. 1e, the clear contrast between the dark skeletons and inner bright regions indicates the formation of bicontinuous nanoporous structure. Similar to the observation from SEM, it is clear that many nanoparticles exist among the interconnected nanoscaled network. And then, high resolution TEM (HRTEM) was further characterized to offer the insight into the structure of Si/Ag composite. Fig. 1f gives the HRTEM image of the part marked by box 1 in Fig. 1e, in which the highly ordered lattice fringes with the lattice spacing of ~0.31 nm are in according with the (111) crystal planes of a well crystallized face-centered cubic (fcc) Si structure. Meanwhile, the HRTEM image of the part marked by box 2 in Fig. 1e is presented in Fig. 1g. The clear lattice fringe has the spacing of ~0.23 nm, which is in agreement with the lattice parameter of Ag (111) crystal planes. Consequently, the nanoparticles can be assigned to the formation of Ag nanoparticles. The electron microscope characterizations indicate that the resulted Si/Ag composite has a unique bimodal porous (BP) structure with the incorporation of Ag nanoparticles into the network backbone. The pore size distribution was also measured by BET method. As presented in Fig. S1, the pore size of Si/Ag composite mainly distributed at ~ 40 nm and ~ 1 μm, which were in good agreement with the bimodal porous structure analyzed by electron microscope. Its surface area was measured to be ~ 20 m^2 g^{-1}.

As stated above, dealloying SiAgAl alloy generates an interesting BP structure, and it is intriguing to explore the effect of Ag absence on the structure formation by dealloying SiAl alloy. Fig. 2 gives the resulted structure by dealloying $Si_{10}Al_{90}$ alloy in 0.1 M HCl solution for 10 h at room temperature. It is clearly observed from the surface SEM image (Fig. 2a) that the resulted sample also has a bulky microscaled structure with interconnected large pores distributed on the surface. Fig. 2b illustrates its more detailed structure, where there is also a second-order nanoporous structure within every large pore. A cross-sectional SEM image (Fig. 2c) further demonstrates that HCl solution had penetrated the whole sample with uniform bicontinuous porosity extending in all dimensions upon

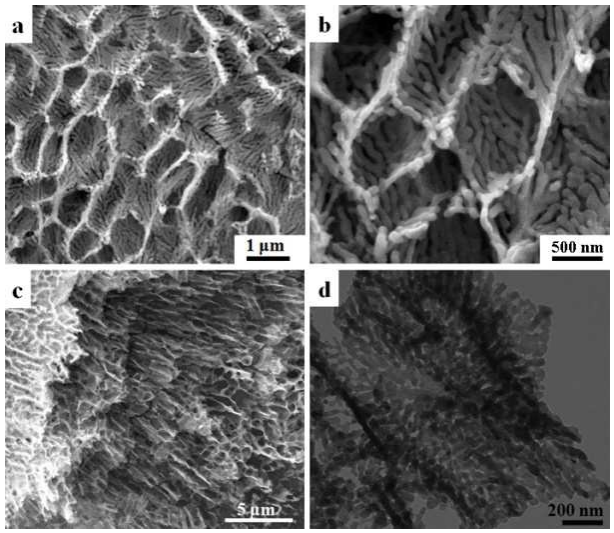

Fig. 2 (a,b) The surface SEM, (c) cross-sectional SEM, and (d) TEM images of the BP Si sample obtained by dealloying $Si_{10}Al_{90}$ alloy in 0.1 M HCl solution for 10 h at room temperature.

dealloying. The detailed structure was further characterized by TEM, in which the interconnected nanoscaled network was clearly observed. Based on the observations above, the as-made Si sample has inherited the BP structure with bimodal pore size distribution. Finally, energy-dispersive X-ray spectrometer (EDS) was carried out to confirm the elementary composition of the BP Si sample. As indicated in Fig. S2, there are Si and Al elements in the sample, but the residual Al is as low as 0.76 at.% (atomic percentage), indicating that most majority of Al atoms have been removed.

The crystal structures of the BP Si and BP Si/Ag samples were examined with the profile of SiAl and SiAgAl alloys included. From the powder X-ray diffraction (XRD) pattern of SiAl binary alloy (Fig. S3a), the diffraction peaks around 28.5, 47.4° and 56.2° (2θ) can be indexed to the fcc structured Si. The diffraction peaks at 38.5°, 44.8°, 65.2°, 78.3° and 82.5° (2θ) can be assigned to Al-like fcc structure. The lattice parameter of the Al-like phase is calculated to be 4.044 Å, which is slightly less than the 4.049 Å of the aluminum powder, indicating the partial solubility of silicon in aluminum.[25-27] In addition, it is noted that the intensity of Si diffraction peaks is much weaker than that of Al-like phase. Therefore, it is possible that less Si is in a phase of pure Si state, and a most majority of Si has incorporated into Al phase to form Al-like fcc structure. Fig. S3b gives the XRD pattern of SiAgAl alloy, which exhibits the similar diffraction peaks to that of SiAl alloy. It is noted that no diffraction peaks can be indexed to metallic Ag, where the Ag atoms may distribute in the crystal lattice of Al-like fcc structure. Upon dealloying, no peak from pure Al is observed in the products (Fig. S3c & S3d). As indicated in Fig. S3c, after dealloying SiAl alloy there is a set of diffraction peaks emerged, which can be indexed to the fcc phase of crystal Si. In the case of Si/Ag composite (Fig. S3d), pure Si

Nanoscale Accepted Manuscript

and Ag can be indexed, which is consistent with the HRTEM observation. EDS measurement (Fig. S4a) indicates that the composition of ternary source alloy has the component of $Si_8Ag_2Al_{90}$, which is highly consistent with our initial feeding ratio in the refining process. Fig. S4b shows that the atomic ratio between Si and Ag upon dealloying is in agreement with that in source alloy, suggesting the good control of the resulted component by dealloying method. Based on the experimental results above, it is concluded that BP Si/Ag composite can be easily fabricated by means of the simple dealloying procedure in terms of controllable bicomponent composition.

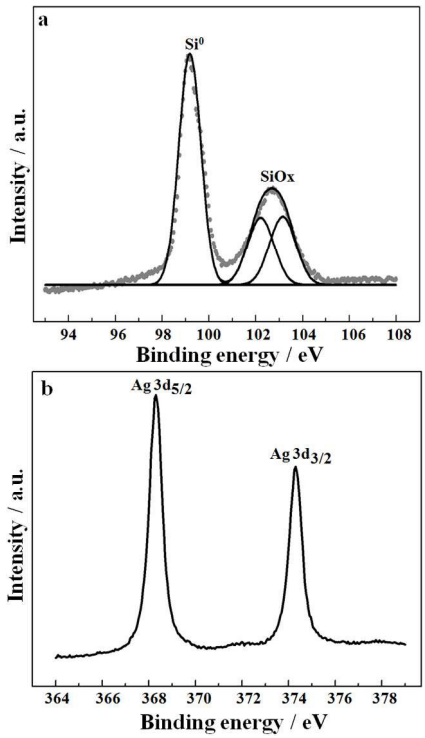

Fig. 3 The XPS spectra of (a) the Si 2p peaks and (b) the Ag 3d peaks of BP Si/Ag composite.

X-ray photoelectron spectrometer (XPS) analysis was further employed to examine the surface properties of the BP Si/Ag composite. As showed in Fig. 3a, the Si 2p spectra shows the presence of elemental Si and oxidation states of Si (Si^{2+} and Si^{4+}) in the BP Si/Ag sample.[28,29] The formation of Si oxides may because that the generated fresh Si atoms upon etching Al easily combine with oxygen during the dealloying and drying process, which is also usually observed in the preparation of other Si materials.[29] Fig. 3b shows the XPS spectra of Ag 3d region, in which the peaks around 368.4 and 374.3 eV can be attributed to metallic Ag,[30] indicating that Ag exists as metallic substance in the BP Si/Ag composite.

The successful fabrication of the pure BP Si and Si/Ag composite provides us a good opportunity to investigate the influence of Ag addition on the structure formation of Si. We monitored the products of dealloying SiAl and SiAgAl alloys during the corrosion process. Fig. 4 firstly presents the SEM images of the sample obtained through dealloying SiAl alloy in different reaction periods. After a short corrosion period of 0.5 h (Fig. 4a), it is found that a certain amount of voids appeared on the original smooth surface of SiAl alloy. When etching SiAl alloy for 1 h (Fig. 4b), some large deep pores formed on the surface (pointed out by arrows). When the corrosion time was extended to 2 h (Fig. 4c), there are more pores emerged.

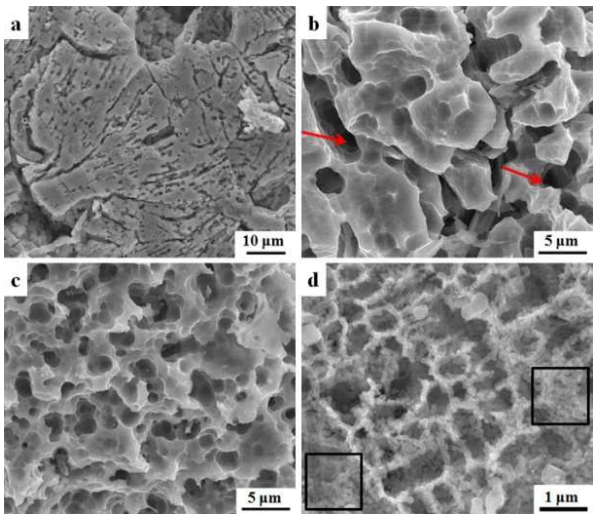

Fig. 4 The SEM images of the products collected by dealloying $Si_{10}Al_{90}$ alloy in 0.1 M HCl solution for (a) 0.5, (b) 1, (c) 2 and (d) 5 h.

For further extending the corrosion time to 5h (Fig. 4d), the first-order large pores and the second-order nanopores can be clearly found. However, the structure at this moment was not uniform (marked by boxes). Finally, a well-defined BP Si formed after dealloying for 10 h (Fig. 2a). Based on the above observations, Al atoms were selectively dissolved gradually with the dealloying time, thus the exposed Si atoms became less coordinated, which grown to form nuclei and self-assembled to form the unique BP structure. Such an etching and crystal growth process should start from the surface of SiAl alloy, and gradually extended to the inner along with the permeation of HCl solution.

Fig. 5 further gives the structure evolution of BP Si/Ag composite in different reaction periods. Fig. 5a gives the SEM image of the sample obtained through dealloying SiAgAl alloy for 2 h. Although some holes formed due to the dissolution of partial Al, the porous structure was quite nonuniform at this stage. When the corrosion time reached 5 h (Fig. 5b), it is discovered that first-order porous backbone had taken shape, and a mass of Ag nanoparticles around 50 nm distributed uniformly in the sample. However, the structure at this moment was defective and some aggregations can be clearly observed, which was similar to the situation of dealloying SiAl alloy for 5 h (Fig. 4d). XRD measurement was also carried out to understand the evolution of crystal structure during the dealloying process. Fig. S5 gives the XRD pattern of the samples obtained by etching in HCl solution for 2 h and 5 h. It is clearly observed that the diffraction peak intensity of Al quickly decreased with the extension of etching time, meanwhile the diffraction peak intensity of Si and Ag became strong. When etching for 10 h, the diffraction peak of Al completely disappeared (Fig. S3d), while the BP Si/Ag structure finally formed.

Nanoscale Accepted Manuscript

This journal is © The Royal Society of Chemistry [year]

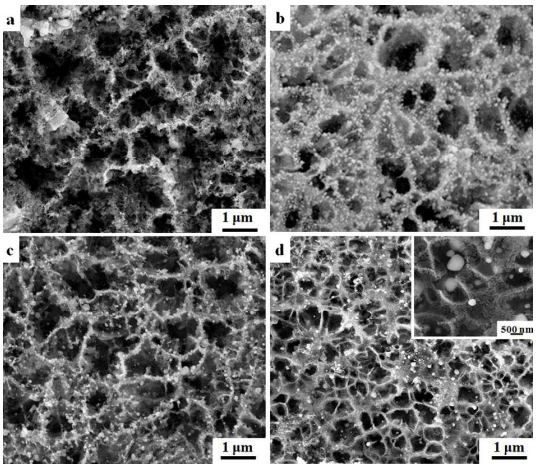

Fig. 5 The SEM images of the products collected by dealloying $Si_8Ag_2Al_{90}$ alloy in 0.1 M HCl solution for (a) 2, (b) 5, (c) 10 and (d) 24 h.

Once etching for 10 h (Fig. 1a & 5c), the well BP structured product was obtained, with Ag nanoparticles less than 100 nm continuously attached on the surface. If the corrosion process was lasted for 24 h (Fig. 5d), the BP structure was still clearly legible, but the distribution of Ag particles became extremely uneven, and some particles had the size even above 500 nm (Fig. 5d inset). Therefore, one can draw a primary conclusion that the longer corrosion process is beneficial to the formation of uniform BP Si structure, but will result in the aggregation of Ag nanoparticles. As stated above, HCl solution is suitable for dealloying SiAl and SiAgAl alloys to fabricate nanoporous materials. It is known that Al is reactive to many common agents as well Si is not etched. Consequently, other chemical agents such as H_2SO_4 and HCOOH solutions were also selected to dealloy the as-made $Si_{10}Al_{90}$ alloys compared with the case in HCl solution. When etching for 2 h (Fig. S6a), all the surface color of alloys in HCl and H_2SO_4 solutions became dark yellow, but more bubbles emerged in HCl solutions than in H_2SO_4 solutions. Once the corrosion time exceeded 5 h (Fig. S6b-d), the alloy foils in HCl solution dissolved gradually and the solution became turbid with deep yellow color. In the case of H_2SO_4 solutions, there was almost no change of experimental phenomenon between 5 to 24 h. These results manifested that it is hard for H_2SO_4 to permeate into the inner of SiAl alloy. As for a weak acid environment of HCOOH solution, there was no evident change of alloy foils from beginning to end. In addition, SEM observation of the product dealloying in 1 M HCl solution for 10 h was conducted to explore the effect of etching solution in high concentration on the dealloying structure. It is observed that the morphology and size of the product were strongly heterogeneous (Fig. S7), indicating a moderately corrosive environment is of importance for the resulted nanostructure.

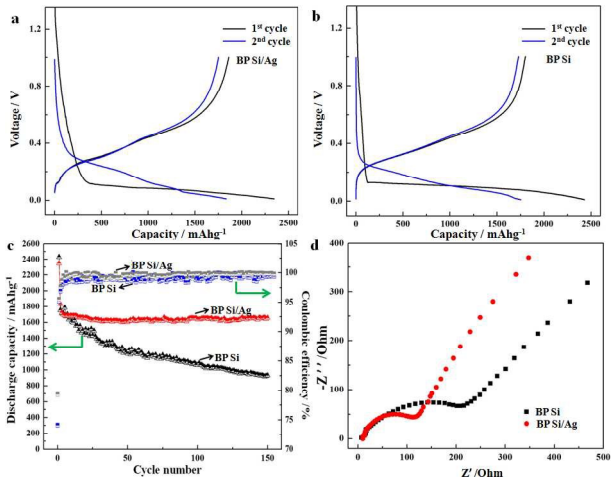

Fig. 6 The (a,b) voltage profiles, (c) cycle performance, and (d) impedance measurements of BP Si and BP Si/Ag electrodes. [The current rate is 200 mA g^{-1}]

The as-made BP Si/Ag composite has the rich porosity and incorporation of well conductive Ag, which are particularly desirable for the highly efficient electrode material for LIBs. Therefore, the BP Si/Ag composite was employed as an active anode material, with pure BP Si included for comparison. Fig. 6a presents the voltage profiles of the BP Si/Ag electrode for the first two cycles at 200 mA g^{-1} between 0.01 and 1 V in a coin-type half cell. The first discharge and charge capacities were 2343.6 and 1860.2 mA h g^{-1}, respectively. The irreversible capacity can be mainly assigned to the decomposition of electrolyte, forming a solid/electrolyte interphase on the electrode surface.[31] In addition, the first discharge curve displayed a long plateau at ~ 0.1 V, indicating a two-phase reaction between the crystalline Si phase and the amorphous LixSi phase.[32] Meanwhile, Fig. 6b gives the electrochemical behavior of the pure BP Si electrode at the same condition. It is found that BP Si had the similar voltage profiles with BP Si/Ag electrode. However, without Ag addition, BP Si delivered a slightly higher initial discharge capacity of 2429.4 mA h g^{-1}.

To clarify the effects of introducing well conductive Ag on the electrochemical performance, we further compared the cycling performances of BP Si/Ag composite with pure BP Si. Fig. 6c presents the cycling capacities and stabilities of both samples at the rate of 200 mA g^{-1}. It is observed that a rapid capacity decay occurred for pure BP Si as the cycling progress, which remained 1061.5 mA h g^{-1} at 100th cycle and 931.5 mA h g^{-1} at 150th cycle, keeping only 43.7 % and 38.3 % of the initial discharge capacity, respectively. However, such the cycling stability is still much higher than that of commercial Si nanoparticles.[11] This should be attributed to its unique BP structure, which offers sufficient void space to accommodate the large volume expansions of silicon and enhances the accessibility of Li^+ and electrolyte.[33] In contrast, BP Si/Ag composite demonstrated a much more superior electrochemical reversibility. As illustrated in Fig. 6c, a capacity of 1656.0 mA h g^{-1} was obtained for BP Si/Ag anode at 150th cycle with no noticeable capacity degradation from the third cycle upwards, leading to the capacity retentions of 70.7 % against the first cycle and 96.1 % against the third cycle. It means that introducing Ag is important here for maintaining the cycling stability of silicon, which generates an enhanced electric

Nanoscale Accepted Manuscript

conductivity and a decreased inner resistance.[11] In addition, the coulombic efficiency (CE) data of both anodes during the discharging-charging cycles were further presented in Figure 6c. It is clear that BP Si anode delivered an initial CE of 74.1%. However, the BP Si/Ag composite presented a higher initial CE of 79.3%, which further increased quickly to 95.5 % at the second cycle, and maintained between 97-100 % during the following cycles. Furthermore, Fig. S8 presents the TEM image of the BP Si/Ag sample after cycling for 150 cycles. It is discovered that the Ag nanoparticles underwent agglomeration to some extent. However, the anode material still kept the initial porous structure except slight coarsening and clogging, which resulted from the repeated lithium ion intercalation and deintercalation. Therefore, the structural stability should be responsible for the well-improved cycling performance.

For the direct verification of the contributions from Ag on the conductivity, fully discharged (0.01V) BP Si/Ag composite and pure BP Si electrodes were analyzed by using electrochemical impedance spectroscopy (EIS) after cycling 150 times at 200 mA g^{-1}. As presented in Fig. 6d, both Nyquist plots consist of a straight line in the low frequency region and a depressed semicircle in the high frequency region. It is noted that the most evident difference between them is the size of the semicircle, which measures the resistance to charge transfer in the electrode. With the introduction of Ag, the impedance of electrode is obviously reduced, which should be mainly attributed to greater electric connectivity of Si by the Ag nanoparticles. The results are consistent with that stated in the earlier researches.[11,12]

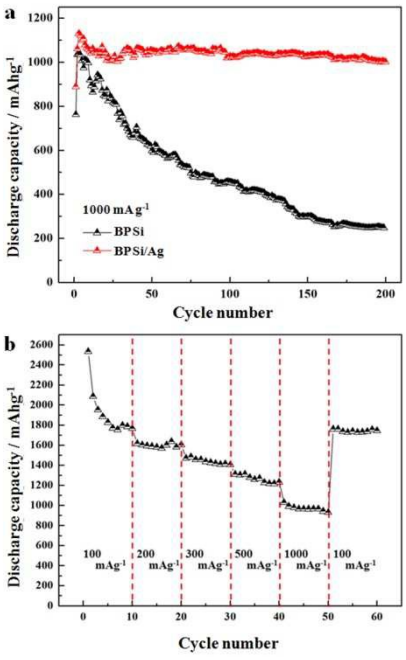

Fig. 7 (a) The cycle performance of BP Si and BP Si/Ag at the rate of 1000 mA g^{-1}, and (b) the rate performance of BP Si/Ag composite.

A good cycling stability at high current rate is another important parameter for an excellent anode material. Therefore, the cycle stability of BP Si/Ag composite was further evaluated under a high current density of 1000 mA g^{-1} with the profile of BP Si included for comparison. As shown in Fig. 7a, for both anodes, the specific capacities of the first two cycles were lower than that of the third cycle, indicating an activation process of electrodes. BP Si anode exhibited a highest capacity of 1037.8 mA h g^{-1} at the third cycle, but a fast capacity fading appeared from then on, resulting in a capacity retention of only 23.9 % at the 200th cycle. In comparison, BP Si/Ag composite demonstrated a high electrochemical reversibility. A highest capacity of 1130.3 mA h g^{-1} was obtained at the third cycle, up to 89.2% of which can be retained at the 200th cycle. It manifests again that Ag introducing is highly effective for improving the cycling stability of Si anode, especially at high rate.

In particular, the BP Si/Ag electrode showed an excellent rate performance, which was evaluated in discrete steps from 100 to 1000 mA g^{-1}. As shown in Fig. 7b, BP Si/Ag composite showed very good cycling stability at each current density. When the current rates were increased from 100 to 200, 300, 500 and 1000 mA g^{-1} in stages, the BP Si/Ag anode delivered the reversible capacities of about 1760, 1600, 1420, 1230 and 960 mA h g^{-1}, respectively. When the current density was set back to 100 mA g^{-1}, a capacity of ~ 1750 mA h g^{-1} could be well recovered, which reached up to 99 % of the capacity at the previous rate of 100 mA g^{-1}. The superiority of BP Si/Ag composite in high power capability is further visualized, which may be attributed to the following reasons.[11,12,21,34-37] First, the micro-sized Si/Ag powders can be packed densely on the current collector, ensuring the electric connectivity. Second, the bimodal porous structure can provide rich porosity, allowing the free expansion of Si with alleviative mechanical constrain during Li alloying and dealloying process, as well facilitating the transport behaviors of Li ions and electrons. Third, the introduction of Ag nanoparticles can bring an efficient electron conducting pathway for Si, etc.

4. Conclusions

BP Si/Ag composite with micro-nano bimodal porous structure and controllable component proportion was easily fabricated through one-step dealloying SiAgAl alloy in mild condition. The as-made BP Si/Ag composite exhibited much improved cycling stability toward lithium storage compared with pure BP Si anode, especially at high current rate. In addition, BP Si/Ag composite also showed an excellent rate capability due to the structural advantage coupled with the introduction of well conductive Ag. The BP Si/Ag composite holds great application potential as an advanced anode material for Li-ion batteries in terms of superior electrochemical performance and easy preparation.

Acknowledgment

The authors would like to express their sincere gratitude to Prof. Xiangfa Liu, Prof. Yuying Wu, and the key laboratory for liquid-solid structural evolution and processing of materials (Ministry of Education, Shandong University). This work was also supported by the National Science Foundation of China (21401074, 21271085).

Notes

School of Chemistry and Chemical Engineering, University of Jinan, Jinan, 250022, China.
Fax: +86-531-82765969

Nanoscale Accepted Manuscript

This journal is © The Royal Society of Chemistry [year]

Tel: +86-531-89736103

E-mail: chm_xucx@ujn.edu.cn

Electronic Supplementary Information (ESI) available: EDS and XRD measurements of the dealloyed products and alloy precursors; Digital photographs of the dealloying experiments of SiAl alloys in different acid solutions; SEM image of the product obtained from etching SiAl alloy in 1 M HCl solution for 10 h. See DOI: 10.1039/b000000x/

References

1. J. B. Goodenough and K. S. Park, J. Am. Chem. Soc., 2013, **135**, 1167.
2. V. Etacheri, R. Marom, R. Elazari, G. Salitra and D. Aurbach, *Energy Environ. Sci.*, 2011,**4**, 3243.
3. J. B. Goodenough, *Energy Environ. Sci.*, 2014, **7**, 14.
4. R. Mukherjee, R. Krishnan, T. M. Lu and N. Koratkar, *Nano Energy*, 2012, **1**, 518.
5. G. Jeong, Y. U. Kim, H. Kim, Y. J. Kim and H. J. Sohn, *Energy Environ. Sci.*, 2011, **4**, 1986.
6. H. Ghassemi, M. Au, N. Chen, P. A. Heiden and R. S. Yassar, *ACS Nano*, 2011, **5**, 7805.
7. X. K. Huang, H. H. Pu, J. B. Chang, S. M. Cui, P. B. Hallac, J. W. Jiang, P. T. Hurley and J. H. Chen, *ACS Appl. Mater. Interfaces*, 2013, **5**, 11965.
8. C. Kim, M. Ko, S. Yoo, S. Chae, S. Choi, E. H. Lee, S. Ko, S. Y. Lee, J. Cho and S. Park, *Nanoscale*, 2014, **6**, 10604.
9. F. F. Cao, J. W. Deng, S. Xin, H. X. Ji, O. G. Schmidt, L. J. Wan, Y. G. Guo, *Adv. Mater.*, 2011, **23**, 4415.
10. H. C.Tao, L. Z. Fan, W. L. Song, M. Wu, X. B. He and X. H. Qu, *Nanoscale*, 2014, **6**, 3138.
11. Y. Yu, L. Gu, C. B. Zhu, S. Tsukimoto, P. A. van Aken and J. Maier, *Adv. Mater.*, 2010, **22**, 2247.
12. D. Y. Chen, X. Mei, Ji, G. M. H. Lu, J. P. Xie, J. M. Lu and J. Y. Lee, *Angew. Chem. Int. Ed.*, 2012, **51**, 2409.
13. X. L. Yang, Z. Y. Wen, S. H. Huang, X. J. Zhu and X. F. Zhang, *Solid State Ion.*, 2006, **177**, 2807.
14. S. Yoo, J. Lee, S. Ko and S. Park, *Nano Energy*, 2013, **2**, 1271.
15. W. J. Zhao, N. Du, C. M. Xiao, H. Wu, H. Zhang, D. R. Yang, *J. Mater. Chem. A*, 2014, **2**, 13949.
16. S. L. Jing, H. Jiang, Y. J. Hu and C. Z. Li, *Nanoscale*, 2014, **6**, 14441.
17. H. P. Jia, P. F. Gao, J. Yang, J. L. Wang, Y. N. Nuli and Z. Yang, *Adv. Energy Mater.*, 2011, **1**, 1036.
18. J. Q. Wang, Y. Yu, L. Gu, C. L. Wang, K. Tang and J. Maier, *Nanoscale*, 2013, **5**, 2647.
19. B. M. Bang, H. Kim, H. K. Song, J. Cho and S. Park, *Energy Environ. Sci.*, 2011, **4**, 5013.
20. M. Y. Wu, J. E. C. Sabisch, X. Y. Song, A. M. Minor, V. S. Battaglia, G. Liu, *Nano Lett.*, 2013, **13**, 5397.
21. Z. H. Bao, M. R. Weatherspoon, S. Shian, Y. Cai, P. D. Graham, S. M. Allan, G. Ahmad, M. B. Dickerson, B. C. Church, Z. T. Kang, H. W. Abernathy III, C. J. Summers, M. L. Liu, K. H. Sandhage, *Nature*, 2007, **446**, 172.
22. B. M. Bang, H. Kim, H. K. Song, J. Cho and S. Park, *Energy Environ. Sci.*, 2011, **4**, 5013.
23. J. Yeom, D. Ratchford, C. R. Field, T. H. Brintlinger and P. E. Pehrsson, *Adv. Funct. Mater.*, 2014, **24**, 106.
24. C. X. Xu, J. X. Su, X. H. Xu, P. P. Liu, H. J. Zhao, F. Tian and Y. Ding, *J. Am. Chem. Soc.*, 2007, **129**, 42.
25. W. C. Zhou, S. Upreti and M. S. Whittingham, *Electrochem. Commun.*, 2011, **13**, 158.
26. Z. B. Sun, X. D.Wang, X. P. Li, M. S. Zhao, Y. Li, Y. M. Zhu and X. P. Song, *J. Power Sources*, 2008, **182**, 353.
27. W. C. Zhou, T. C. Jiang, H. Zhou, Y. X. Wang, J. Y. Fang and M. S. Whittingham, *MRS Commun.*, 2013, **3**, 119.
28. D. B. Polat, O. Keles and K. Amine, *J. Power Sources*, 2014, **270**, 238.
29. S. Guo, H. X. Li, H. M. Bai, Z. L. Tao and J. Chen, *J. Power Sources*, 2014, **248**, 1141.
30. Z. M. Liu, N. Q. Zhang, Z. J. Wang and K. N. Sun, *J. Power Sources*, 2012, **205**, 479.
31. H. Kim, M. Seo, M. H. Park and J. Cho, *Angew. Chem. Int. Ed.*, 2010, **49**, 2146.
32. C. K. Chan, H. Peng, G. Liu, K. McIlwrath, X. F. Zhang, R. A. Huggins and Y. Cui, *Nat Nanotechnol.*, 2008, **3**, 31.
33. H. Kim, B. Han, J. Choo and J. Cho, *Angew. Chem. Int. Ed.*, 2008, **47**, 10151.
34. H. Liu, L. B. Hu, Y. S. Meng and Q. Li, *Naonoscale*, 2013, **5**, 10376.
35. J. Z. Chen, L. Yang, S. Rousidan, S. H. Fang, Z. X. Zhang and S. Hirano, *Nanoscale*, 2013, **5**, 10623.
36. J. P. Li, P. Wu, Y. W. Tang, X. L. Xu, Y. M. Zhou, Y. Chen and T. H. Lu, *CrystEngComm*, 2013, **15**, 10340.
37. P. Wu, H. Wang, Y. W. Tang, Y. M. Zhou and T. H. Lu, *ACS Appl. Mater. Interfaces*, 2014, **6**, 3546

Nanoscale Accepted Manuscript

Table of Contents Graphic and Summary

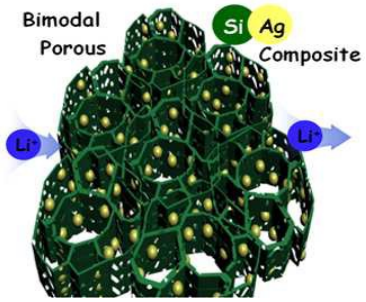

Bimodal porous Si/Ag composite is easily fabricated by etching SiAgAl alloy in HCl solution, and performs excellently for lithium storage.

Nanoscale Accepted Manuscript

This journal is © The Royal Society of Chemistry [year]